Research Square

Preprints are preliminary reports that have not undergone peer review.
They should not be considered conclusive, used to inform clinical practice,
or referenced by the media as validated information.

Construct validity and evidence boundaries of a 17-gene transcriptomic proxy for mitoxyperilysis in colorectal aging and cancer Analysis

Pan Sun
Guizhou Medical University
Jinglin Wang
Guizhou Medical University
Yao Wang
Guizhou Medical University
Yan Zhang
Guizhou Medical University
Yao Tang
Guizhou Medical University
Juan Yang
yj63yj63@163.com
Guizhou Medical University
Zejun Wang
Guizhou Medical University

Research Article

Keywords: mitoxyperilysis, colorectal cancer, cellular senescence, transcriptomic proxy, single-cell RNA sequencing, pharmacogenomics, construct validity

Posted Date: September 15th, 2026

DOI: https://doi.org/10.21203/rs.3.rs-10804793/v1

License: This work is licensed under a Creative Commons Attribution 4.0 International License.
Read Full License

Additional Declarations: No competing interests reported.

Abstract

Mitoxyperilysis is a recently described lytic cell-death process defined by prolonged mitochondria–plasma-membrane contact, localized oxidative injury, and membrane rupture under combined innate-immune and metabolic stress. We evaluated the construct validity of a 17-gene transcriptomic proxy across perturbation, aging, colorectal cancer (CRC), independent senescence measures, genetics, prognosis, and pharmacogenomics. Public datasets were reanalyzed with culture-, donor-, patient-, pair-, or cell-line-level inference, multiplicity control, cell-composition sensitivity, and cross-platform evaluation. All 17 genes responded to combined stress in GSE235046, but the directions and Torin responses were mixed. In GTEx colon, the proxy–age association attenuated after adjustment (Spearman rho 0.125 to 0.052). In GSE44076, proxy–senescence covariance was inverse in healthy mucosa (rho − 0.324), absent in adjacent mucosa, and positive in tumor (rho 0.354), without a paired proxy increase. Bulk CRC covariance replicated across cohorts (random-effects rho 0.339, 95% CI 0.172–0.486) and persisted after cell-composition adjustment. An exploratory CPTAC-2 reduced-feature check showed protein-layer covariance using 10/17 proxy and 8/12 reference genes (rho 0.292, P = 0.0037). However, none of seven panel-disjoint patient-level tests using two independent senescence algorithms met predefined validation criteria. The panel did not overlap 208 prioritized CRC effector genes; adjusted survival and observed drug-response analyses were null. Thus, this context-sensitive proxy is not a validated measure of mitoxyperilysis, senescence, inherited risk, prognosis, or drug sensitivity. Direct validation requires colorectal-relevant perturbation and rescue linked to spatial, oxidative, and membrane-integrity phenotypes.

1. Introduction

Colorectal cancer (CRC) incidence rises sharply with age, against a background of altered epithelial homeostasis, immune signaling, stromal remodeling, mitochondrial function, and nutrient sensing [1, 2]. Cellular senescence is one component of this age-associated tissue environment. Senescent cells are characterized by durable proliferative arrest and may acquire a senescence-associated secretory phenotype (SASP), but no single transcriptomic marker or short gene set uniquely identifies the state [3–5]. In tumors and inflamed tissues, cytokines commonly used in senescence scores may instead reflect acute innate activation, wound responses, cell composition, or malignant-state programs. Consequently, transcriptomic covariance with a SASP-heavy score is not equivalent to direct evidence of cellular senescence.

Mitoxyperilysis was recently described as a lytic cell-death outcome of combined innate-immune activation and metabolic disruption [6–9]. In the defining experiments, damaged mitochondria remained in prolonged contact with the plasma membrane, generating localized oxidative damage through a process termed mitoxyperiosis; membrane permeabilization, bursting, and lytic death followed. BAX, BAK1, BID, mTORC2-dependent positioning, oxidative stress, and cytoskeletal dynamics contributed to the phenotype [8]. These properties distinguish a spatially gated death process from a transcriptional

pathway score. Neither bulk RNA sequencing nor ordinary single-cell RNA sequencing records mitochondria–membrane proximity, local lipid oxidation, membrane rupture, or death itself.

The novelty of a biological term creates a predictable bioinformatic risk: genes mentioned in the mechanism can be assembled into a score before the score has been validated against the defining phenotype. Such a quantity may be useful as a hypothesis-generating transcriptional proxy, but it becomes circular if its association with another score derived from the same expression matrix is presented as proof of the mechanism. The risks are amplified by pseudo-replication in single-cell data, anatomical mixing, arbitrary score direction, outcome-optimized cutoffs, or drug-response values predicted from the same tumor-expression input.

A recent CRC study linked a mitoxyperilysis-related expression signature with prognosis, immune remodeling, and tumor ecology [10]. Here, we addressed three narrower questions: (i) do the 17 candidate genes respond coherently to the defining perturbation and rescue; (ii) is covariance with senescence-associated transcription reproducible across anatomy and platform, and retained with independent senescence constructs at the donor or patient level; and (iii) does the proxy generalize to genetic, survival, or observed pharmacogenomic endpoints? Same-matrix covariance was considered descriptive, whereas orthogonal senescence algorithms, patient-level single-cell inference, external CRC genetics, observed cell-line drug response, and adjusted survival were used for triangulation. We did not perform PC1-based ‘pseudotime,’ an uncalibrated transcriptomic aging-clock analysis, composite-score Mendelian randomization, observational virtual perturbation, or coordinate-free spatial analysis because the available data did not support identifiable or independently testable estimands.

2. Materials and methods

2.1 Study design, evidence hierarchy, and independent units

This retrospective multi-cohort study used public, de-identified data and a predefined evidence hierarchy: perturbational responsiveness; donor-level normal-colon and corrected mucosal context; bulk-tumor replication; patient-level, panel-disjoint senescence testing; and clinical, genetic, and observed pharmacogenomic triangulation. The inferential unit was the culture/sample in GSE235046, donor in GTEx, participant or matched pair in GSE44076, patient in TCGA/GSE39582, patient/specimen profile in GSE132465, and cell line in GDSC2. Cells were nested measurements, not biological replicates. Multiple-testing families used BH correction [11]. Analysis families and decision criteria were frozen in an internal analysis contract before the final sensitivity analyses; the study was not prospectively preregistered. The complete sequence and decision criteria are provided in Supplementary Information 1, Supplementary Method 1.

2.2 Datasets and assigned roles

GSE235046 provided a murine bone-marrow-derived macrophage perturbation model with media, lipopolysaccharide (LPS), carbon starvation, combined LPS plus carbon starvation, and combined stress plus Torin conditions. GTEx supplied normal human sigmoid and transverse colon tissue [12]. TCGA-COAD and TCGA-READ tumors were obtained through UCSC Xena [13, 14]. GSE63577 contained five fibroblast strains across replicative population doublings [15]; GSE132465 comprised 63,689 annotated cells from 23 patients and 33 specimens [16]; GSE39582 contained 585 CRC microarrays with follow-up [17]; and GSE44076 contained 50 lesion-free healthy mucosa samples and 98 paired adjacent-mucosa/tumor samples [18].

Pharmacogenomic analyses used official GDSC2 matrices distributed with oncoPredict [19–21]. Orthogonal senescence analyses used the official hUSI and SenePy implementations [22, 23]. The genetic target set came from the official Law et al. CRC fine-mapping workbook [24]. Each cohort had one principal evidential role; alternative normalizations or regroupings were sensitivities rather than independent replications.

2.3 Candidate genes and score construction

The 17 genes were BAK1, BAX, BID, MTOR, MYD88, NFE2L2, NINJ1, NLRP3, RHOA, RICTOR, RPTOR, TLR2, TLR4, TLR7, TLR8, TNFRSF1A, and TNFRSF1B. These genes were selected by the authors from the emerging mechanism literature and prior analytical work; they were not derived by outcome optimization in the cohorts analyzed here. The panel was evaluated as an author-curated proxy and was not treated as a direct reproduction of the prognostic expression signature reported in reference 10.

Within each dataset, retained expression values were standardized gene-wise across the eligible samples unless a normalization-scope sensitivity was explicitly specified. The primary uniform proxy was

> proxy = (1/G) × Σ z(g),

where G was the number of available candidate genes and z(g) was standardized expression of gene g. A secondary perturbation-weighted proxy was

> weighted proxy = Σ[z(g) × w(g)] / Σ|w(g)|,

where w(g) was the GSE235046 combined-stress-versus-media log2 fold change. Because these weights came from murine macrophages and combined multiple biological effects, the weighted score was treated only as a sensitivity analysis.

The legacy senescence-associated reference score was the mean standardized expression of CDKN1A, CDKN2A, GLB1, IL6, CXCL8, IL1A, IL1B, CCL2, MMP3, SERPINE1, and TGFB1 minus standardized LMNB1. It was used to reproduce and test the original same-expression covariance, not to diagnose senescence. MKI67 was analyzed separately as a proliferation covariate.

2.4 Perturbational reanalysis of GSE235046

Raw counts from 15 profiles (three per condition) were restricted to protein-coding genes, with duplicate symbols summed. After edgeR filtering and TMM normalization, limma-voom modeled a no-intercept condition design with robust empirical-Bayes moderation. The three prespecified estimands were combined LPS plus carbon starvation versus media; the factorial interaction (combined stress − LPS − carbon starvation + media); and Torin-treated versus untreated combined stress. BH correction was applied across the 17 genes within each contrast [11]. Because this perturbation dataset informed the biological provenance of the panel, the analysis was a provenance and perturbational-responsiveness check rather than an independent validation of the panel.

2.5 GTEx donor-level site, normalization, and age analyses

Eligible sigmoid and transverse-colon specimens were scored and aggregated within donor (555 donors overall; 373 sigmoid and 406 transverse). Gene-wise standardization used either all GTEx tissues, reproducing the legacy workflow, or colon only. Spearman estimates used donor-bootstrap confidence intervals; partial-rank models adjusted proxy–reference associations for MKI67, age-bin midpoint, sex, and, when applicable, sampled-site count. Proxy–age models adjusted for MKI67, sex, and sampled-site count, with BH correction within the prespecified age family.

2.6 GSE44076 probe aggregation and tissue-context analysis

Ambiguously mapped probes were removed; eligible probes for each gene were standardized and averaged. This replaced an order-dependent overwrite affecting 23 of the 30 genes used across the two scores. Correlations were estimated separately in unrelated lesion-free healthy mucosa, adjacent mucosa, and tumor, with partial adjustment for available age, sex, and location. Fisher-z correlation differences formed one corrected family. Tumor–adjacent comparisons were paired by participant; healthy donors were unrelated to CRC cases.

2.7 Replicative-senescence sensitivity in GSE63577

The proxy and legacy reference were calculated in BJ, HFF, IMR90, MRC-5, and WI-38 fibroblasts. Within-strain slopes against population doubling were estimated. A strain-stratified permutation test assessed whether the proxy showed a consistent replicative trajectory across the five strains. This experiment was treated as a construct-sensitivity model rather than as direct validation of mitoxyperilysis.

2.8 Bulk CRC covariance and survival

Only one eligible primary tumor per patient was retained from TCGA; sample-type code 01 defined primary tumor. GSE39582 probes were collapsed to gene level before scoring. Same-expression proxy–reference covariance was summarized with Spearman rho and 95% bootstrap confidence intervals. Composition sensitivity used EPIC deconvolution [36] with the built-in reference profile on TCGA-COAD/READ (Xena HiSeqV2, log2-transformed to linear scale) and GSE39582 (GPL570 probes collapsed to genes via hgu133plus2.db, multi-gene probes removed and within-gene probe averages taken); partial-rank models adjusted the covariance for MKI67, immune fraction, fibroblast fraction, and a purity proxy.

Cross-cohort synthesis used Fisher-z random-effects meta-analysis (DerSimonian–Laird) with I^2 and Q tests across TCGA-COAD, TCGA-READ, GSE39582, and GSE44076 tumors; the nested combined COADREAD cohort was excluded from the primary meta-analysis. Leave-one-gene-out re-scoring recomputed the uniform proxy after deleting each of the 17 panel genes in turn and repeated the TCGA covariance from the same frozen score table; full-panel reference estimates under this pipeline (COAD rho = 0.423; READ rho = 0.439) matched the bootstrap-based summaries in Section 3.4 (0.424 and 0.431) within rounding.

OS and relapse-free survival (RFS) were modeled with continuous scores standardized to one sample standard deviation. Complete-case Cox models used robust variance and adjusted for available age, sex, stage, and MKI67. Proportional hazards were checked with rank-transformed Schoenfeld-residual tests when events allowed; BH correction was applied across prespecified score-by-endpoint families.

2.9 Patient-aware single-cell pseudobulk analysis

GSE132465 UMI counts were joined to author annotations, library-size normalized, and log transformed. Scores were summarized within sample-by-broad-cell-type profiles; inferential sample sizes were determined by patients/specimens. Tumor profiles required at least 20 cells. A sensitivity analysis removed cells with fewer than two detected legacy-reference genes. Pooled-cell results were descriptive only; patient-level bootstrap and leave-one-patient-out analyses assessed stability.

2.10 Orthogonal senescence validation with hUSI and SenePy

The official hUSI and SenePy implementations were version-pinned before analysis [22, 23]. All 17 candidate genes were removed from every senescence construct before scoring. hUSI was calculated for epithelial, myeloid, stromal, T-cell, and B-cell tumor profiles as the Spearman correlation between the official OCLR weight vector and log-normalized pseudobulk expression; 12,896 hUSI features remained after panel removal and detection filtering. SenePy used its official cell-level default—binary gene detection, expression-matched backgrounds, and hub-importance weights—followed by averaging within sample-by-cell-type profiles. Prespecified cell-type mappings were human intestine/epithelial cell for epithelial profiles and human intestine/macrophage for myeloid profiles.

Five hUSI and two SenePy tests formed one BH-corrected family. QC models controlled for cell count, median UMI count, and detected genes; full models added MKI67 and an inflammatory-expression covariate. Robustness analyses used 2,000 resamples, leave-one-patient-out estimates, and 1,000 expression/detection-matched 17-gene panels. Validation required $q < 0.05$ after full adjustment, direction retention in at least 90% of patient deletions, and empirical matched-panel $q < 0.05$.

2.11 CRC genetic-target projection

The SHA-256-verified Law et al. workbook was parsed according to its published target-gene table [24]. After delimiter handling, deduplication, and the documented COLCA2→POU2AF3 alias, the inventory

contained 208 genes (117 high confidence). Direct overlap and full-set/high-confidence expression projections were tested in five tumor compartments using the single-cell QC, covariate, resampling, leave-one-patient-out, and 1,000 matched-gene-set procedures. These were expression projections, not polygenic risk scores or causal estimates.

2.12 Observed pharmacogenomics and oncoPredict diagnostics

The official oncoPredict repository (commit c16c1ffaffdd855f4ada4c83a3948e5c16b618c5) and SHA-256-verified GDSC2 archive provided expression for 805 cell lines and ln(IC50) for 198 drugs. Forty-six CRC lines were eligible, and 185 drugs had at least 20 observed responses. Eight drugs were predefined for the final analysis. Observed-response models retained the official ln(IC50) scale and used raw and partial Spearman estimates adjusted for expression PC1, MKI67, and general drug response, with BH correction, bootstrap, and leave-one-line-out analyses.

Leakage-safe ten-fold oncoPredict evaluation preceded TCGA application. For this model evaluation, the official ln(IC50) values were exponentiated to a positive raw-IC50 scale; oncoPredict applied its within-training-fold power transformation and returned predictions after inverse transformation. Spearman rho and q therefore assessed rank performance, whereas normalized RMSE and out-of-fold R2 described calibration on the raw-IC50 scale and are not ln(IC50)-scale error measures. A predefined rank criterion of rho ≥ 0.30 and q < 0.05 did not imply absolute calibration. TCGA predictions used the same raw-IC50 modeling scale. TCGA associations were interpretable only with model performance, observed CRC-line support, direction agreement, multiplicity control, and global-state adjustment. Otherwise, correlations between two expression-derived quantities were treated as shared-input diagnostics.

2.13 Algebra audit and estimand-based analysis exclusions

Earlier epithelial, myeloid, and stromal weights were tested algebraically. Their gene-wise sum was zero, matrix rank was two, and sample scores summed to zero to numerical precision; they were dependent contrasts rather than three independent programs. Analyses without identifiable or independently testable estimands were not performed. The data-specific rationale for excluding PC1-based temporal claims, an uncalibrated aging clock, composite-score Mendelian randomization, observational virtual perturbation, and coordinate-free spatial analysis is provided in Supplementary Information 1, Supplementary Method 9 [25, 26].

2.14 Statistical reporting and reproducibility

Tests were two sided. Machine-readable tables retained effect sizes, denominators, confidence intervals where estimable, raw P values, and BH q values; no outcome-optimized threshold was used. Scripts recorded software sessions, input hashes, external-code commits, seeds, and figure source data. Independent reanalysis produced identical hashes for 41 overlapping result files. Software versions are detailed in the reproducibility package.

2.15 Cross-platform and dependency checks

An exploratory reduced-feature modality check used the CPTAC-2 prospective colon cohort (cBioPortal study coad_cptac_2019; 110 samples) [37]. Of the prespecified genes, 10/17 proxy genes and 8/12 legacy-reference genes were measurable at the protein layer. Reduced-feature mRNA and protein summaries were constructed from the available features, and sample-level Spearman tests assessed within-layer proxy–reference covariance. Per-gene mRNA–protein concordance used available paired observations, whose sample sizes varied by gene. Because protein missingness was heterogeneous and the scoring implementation did not enforce a fixed per-sample coverage threshold, this analysis was considered an exploratory modality-sensitivity check rather than independent construct validation. CRISPR dependency was assessed in DepMap 24Q2 (CRISPRGeneEffect; 61 CRC cell lines) with CERES < − 0.5 defined as dependency, compared against the full-lineage background [38]. Protein evidence and RNA tissue distribution for the 17 panel genes were retrieved from Human Protein Atlas JSON summaries [39].

3. Results

3.1 Perturbation supports transcriptional responsiveness but not a coherent activity-and-rescue signature

All 17 candidate genes changed under combined LPS plus carbon starvation relative to media after panel correction: 13 increased and 4 decreased (Fig. 1a). Factorial interactions were supported for 15/17 genes—11 positive and 4 negative (Fig. 1b). Torin changed 16/17 genes, with 8 increasing and 8 decreasing; NINJ1 was unchanged (Fig. 1c,D). Among genes previously highlighted by an ad hoc positive rule, BID, NLRP3, and TNFRSF1B decreased after Torin, RICTOR, TLR2, and TLR7 increased, and NINJ1 was unchanged. Thus, GSE235046 established component-gene responsiveness in murine macrophages but did not support a coherent direction, uniform rescue, or a calibrated human CRC activity score.

3.2 Normal-colon covariance depends on anatomy and standardization, while the age association attenuates

Across 555 donor-aggregated GTEx colon profiles, the proxy correlated with the legacy senescence-associated reference (rho = 0.324, 95% CI 0.247–0.396; adjusted rho = 0.237, $P = 1.59 \times 10^{-8}$). Site estimates depended on the z-score reference: with all-GTEx standardization, adjusted rho was − 0.010 ($q = 0.843$) in sigmoid and 0.401 ($q = 1.11 \times 10^{-16}$) in transverse colon; with colon-only standardization, it was 0.215 ($q = 3.98 \times 10^{-5}$) and 0.516 ($q = 3.86 \times 10^{-28}$), respectively (Fig. 2a,D). The persistence of a larger transverse estimate did not remove the scoring-scope dependence. Neither strict transverse specificity nor anatomical equivalence was stable across definitions.

The proxy–age estimate attenuated from rho = 0.125 (q = 0.003) to partial rho = 0.052 (q = 0.222) after adjustment for MKI67, sex, and sampled-site count (Fig. 2b). The legacy reference retained an adjusted association (rho = 0.147, q = 0.001; Fig. 2c). These data did not support use of the proxy as an aging clock or age-acceleration measure.

3.3 Corrected external mucosal data show a context-dependent correlation-sign difference, not a temporal sequence

Correct multi-probe aggregation materially changed GSE44076. In 50 unrelated lesion-free healthy mucosa samples, proxy–reference covariance was inverse (rho = -0.324, q = 0.046); the age-, sex-, and location-adjusted estimate was similar but narrowly missed multiplicity support (partial rho = -0.323, q = 0.058; Fig. 3a,B). Adjacent mucosa from 98 CRC cases showed no association (rho = -0.012, q = 0.930). Tumors from the same 98 cases showed positive covariance (rho = 0.354, q = 0.0010; adjusted rho = 0.350, q = 0.0015). The healthy-versus-tumor difference in Fisher-z-transformed correlations was significant ($q = 3.75 \times 10^{-4}$; Fig. 3c).

Within 98 matched tumor–adjacent pairs, neither the uniform proxy (median change = -0.024, q = 0.492) nor its weighted sensitivity (0.069, q = 0.077) increased convincingly; the legacy reference decreased (-0.546, $q = 1.64 \times 10^{-4}$; Fig. 3d). Because healthy donors were unrelated to CRC cases, the supported result is a cross-sectional disease-context difference in covariance, not an ordered temporal sequence.

3.4 Bulk CRC covariance replicates but does not generalize to orthogonal patient-level senescence measures

Positive same-expression covariance was reproducible across bulk CRC cohorts (Fig. 4a). The uniform proxy correlated with the legacy reference in TCGA-COAD primary tumors (n = 286; rho = 0.424, 95% CI 0.322–0.520), TCGA-READ primary tumors (n = 94; rho = 0.431, 95% CI 0.228–0.611), combined TCGA-COADREAD (n = 380; rho = 0.423), GSE39582 (n = 585; rho = 0.161, 95% CI 0.081–0.239), and GSE44076 tumors (n = 98; rho = 0.354). These replications establish bulk-tumor covariance between two quantities calculated from the same expression matrix; they do not independently identify either mitoxyperilysis or senescence. Across the four non-nested bulk CRC cohorts, the random-effects pooled rho was 0.339 (95% CI 0.172–0.486) with substantial heterogeneity ($I^2 = 85.1\%$, Q-test P = 0.0002; Supplementary Fig. S8), quantifying replication without implying a homogeneous effect. Leave-one-gene-out re-scoring left the TCGA covariance positive in all 17 deletions (COAD range rho = 0.400–0.450; READ 0.394–0.486; maximal absolute change 0.027 and 0.047; Supplementary Fig. S10), indicating that no single panel gene drove the association. After EPIC-based adjustment for immune fraction, fibroblast fraction, and a purity proxy, the covariance remained significant in TCGA-COAD (rho = 0.260, $P = 1.0 \times 10^{-5}$) and TCGA-READ (rho = 0.263, P = 0.012) and was unchanged in GSE39582 (rho = 0.161, $P = 9.3 \times 10^{-5}$), indicating that cell-composition differences do not fully account for the association and that the composition contribution is cohort-dependent (Supplementary Fig. S9; Supplementary Data 1, Table S14).

The replicative-fibroblast model separated the constructs. In GSE63577, the legacy reference increased with population doubling (rho = 0.652; strain-stratified $P = 9.999 \times 10^{-5}$), whereas the proxy was inconsistent across strains (rho = -0.219; stratified P = 0.436; Supplementary Fig. S2).

GSE132465 contained 63,689 cells from only 23 patients. After filtering and patient-level pseudobulk aggregation, proxy–legacy-reference associations were unsupported in epithelial (rho = -0.291, q = 0.357), myeloid (rho = 0.157, q = 0.569), and stromal profiles (rho = 0.203, q = 0.531). In tumor-only sample-level profiles, estimates ranged from rho = -0.277 in stroma to rho = 0.343 in myeloid cells, but no compartment survived correction (all q ≥ 0.592; Supplementary Fig. S3). A stromal association observed without the detection filter did not persist in the filtering sensitivity.

Panel-disjoint hUSI and SenePy analyses likewise did not meet the prespecified validation criterion (Fig. 4b–D). The epithelial hUSI estimate (n = 22; raw rho = 0.502, q = 0.121) attenuated after QC, MKI67, and inflammation adjustment (rho = 0.090, q = 0.927; empirical q = 0.545). Epithelial SenePy changed direction from raw rho = -0.354 (q = 0.331) to adjusted rho = 0.403 (q = 0.628; empirical q = 0.545). None of seven tests satisfied multiplicity, full adjustment, leave-one-patient-out stability, and matched-null specificity. Bulk legacy covariance therefore did not generalize to these external patient-level senescence definitions.

3.5 Cross-platform checks reveal partial protein-layer covariance without CRC-specific dependency

Reduced-feature summaries in CPTAC-2 showed positive within-layer proxy–reference covariance at the protein level (n = 97; rho = 0.292, P = 0.0037) and at the mRNA level (n = 106; rho = 0.318, P = 0.0009). Only 10/17 proxy genes and 8/12 legacy-reference genes were measurable at the protein layer, and per-gene paired mRNA–protein sample sizes ranged from 5 to 96. Among 18 genes measurable at both layers, mRNA–protein concordance varied from rho = − 0.09 to 0.75 and was near zero for MTOR, RICTOR, and RPTOR. This result is an exploratory reduced-feature, same-matrix modality check and not independent validation of the transcriptomic construct. In DepMap 24Q2, none of the 17 panel genes showed CRC-specific CRISPR dependency: dependency was concentrated in MTOR (96.7% of 61 CRC lines), RPTOR (83.6%), and RICTOR (44.3%), at frequencies similar to the full-lineage background. Fifteen of 17 genes have Human Protein Atlas protein-level evidence in human tissues; NLRP3 remains supported only at the transcript level (Supplementary Fig. S11).

3.6 Survival and dependent compartment contrasts provide no independent biomarker support

The uniform proxy was not prognostic in adjusted continuous-score models (Fig. 5a). Adjusted OS estimates were HR = 0.970 per SD in TCGA-COAD (n = 275, 68 events; 95% CI 0.736–1.279; q = 0.996) and HR = 1.046 in GSE39582 (n = 572, 190 events; 95% CI 0.897–1.220; P = 0.566); adjusted GSE39582 RFS was HR = 1.055 (n = 535, 147 events; 95% CI 0.880–1.264; P = 0.563). TCGA-READ had only 17 OS events and a non-null proportional-hazards diagnostic, precluding a stable adjusted claim.

An earlier epithelial-weighted GSE39582 OS association was sensitive to modeling. Its univariable estimate was HR = 0.800 per SD (95% CI 0.699–0.916; q = 0.0127), but adjustment for age, sex, stage, and the prespecified covariates attenuated it to HR = 0.874 (95% CI 0.760–1.005; P = 0.059, q = 0.322). Adjusted RFS was also null (HR = 0.899, 95% CI 0.763–1.060; P = 0.205, q = 0.493; Supplementary Fig. S4).

The epithelial, myeloid, and stromal weight vectors also summed to zero gene-wise, had matrix rank two, and generated sample scores with a zero sum (Supplementary Fig. S1). They were dependent compositional contrasts, not three independent pathway activities.

3.7 CRC target-gene projection does not establish a genetic bridge

The official 2024 CRC resource yielded exactly 208 prioritized effector genes after the documented COLCA2→POU2AF3 alias reconciliation, including 117 high-confidence genes [24]. None directly overlapped the 17-gene panel (0/17; hypergeometric P = 1; Fig. 5b). Of the 208 genes, 175 were detected after disjointing; 106/117 high-confidence genes were detected.

The full 208-gene T-cell projection associated with the proxy (adjusted rho = 0.699, q = 0.00419; empirical q = 0.00999), but the corresponding high-confidence projection was not more specific than matched random sets (adjusted rho = 0.643, q = 0.00999; empirical q = 0.202; Supplementary Fig. S5). Other compartment/target-set tests did not meet the complete criterion. The absence of direct panel overlap and loss of high-confidence specificity precluded a robust genetic anchor; these expression projections are not polygenic risk scores, Mendelian-randomization estimates, or evidence of inherited risk.

3.8 Observed CRC pharmacogenomics provides no support for virtual drug sensitivity

In 46 GDSC2 CRC cell lines, neither proxy associated with observed ln(IC50) for any of eight prespecified drugs after adjustment and multiplicity control (Fig. 5c); the all-drug screen yielded 0/185 supported associations for either proxy (Supplementary Fig. S6).

Ten-fold oncoPredict testing met the rank criterion for 5-fluorouracil, irinotecan, both oxaliplatin models, rapamycin, OSI-027, and Nutlin-3a (rho = 0.522–0.766), but not AZD8055 (rho = 0.089, q = 0.396). Among rank-passing models, normalized RMSE was 0.90–1.00 and out-of-fold R2 was 0.001–0.185, indicating that rank discrimination did not translate into precise absolute prediction (Supplementary Fig. S7).

Several TCGA predicted-response correlations persisted after global-state adjustment, but none had multiplicity-supported observed CRC-line anchoring. Consequently, no proxy-by-drug combination met the integrated evidence criterion (Fig. 5d), and patient sensitivity, resistance, treatment benefit, or a mitoxyperilysis-linked drug mechanism could not be inferred.

4. Discussion

4.1 Principal findings

This study treated the 17-gene quantity as a candidate construct rather than assuming that an expression summary measured the defining phenotype. Construct validity requires convergent evidence together with discriminant tests and external anchors [27, 28]. The genes were perturbation responsive, bulk proxy–reference covariance replicated across CRC cohorts, and GSE44076 showed a supported healthy-versus-tumor correlation difference. However, perturbational directions were mixed, Torin did not produce coherent reversal, and the mucosal comparison was cross-sectional.

The boundaries were consistent across independent tests. The GTEx age association attenuated after adjustment; replicative fibroblasts supported the senescence reference but not a common proxy trajectory; and patient-level hUSI/SenePy results did not reproduce the bulk relationship [22, 23]. Adjusted survival, high-confidence genetic specificity, and observed CRC pharmacogenomics likewise provided no independent confirmation. Composition-adjusted covariance persisted in TCGA and was unchanged in GSE39582. The CPTAC-2 analysis showed positive covariance in a reduced protein feature set, but heterogeneous missingness and partial panel coverage precluded treating it as independent construct validation. The supported construct is therefore a context-sensitive transcriptional proxy, not a measure of the spatial lytic event or a clinical biomarker.

The three prespecified questions therefore have distinct answers. The components respond to the relevant perturbation, but not as a unidirectional induction-and-rescue program. Association with senescence-related transcription is reproducible within bulk CRC yet varies across normal-colon anatomy, scoring reference, and mucosal context, and it is not retained with patient-level panel-disjoint scores. Finally, the available datasets do not show transport to adjusted prognosis, a specific high-confidence CRC genetic projection, or observed drug response. This pattern is more informative than a single positive or negative label because it separates responsiveness, covariance, and external validity.

These evidence levels should not be conflated. Perturbational responsiveness asks whether the selected genes are sensitive to a relevant experimental condition. Convergent covariance asks whether the proxy tracks a related transcriptional construct across settings. Criterion validity would require agreement with the defining spatial, oxidative, and lytic phenotype, and clinical validity would require reproducible association with a patient endpoint beyond routine covariates. The present datasets address the first two levels incompletely and do not contain a criterion-standard human phenotype. The title and conclusions therefore use “proxy” and “construct validity” rather than “activity score,” “signature of occurrence,” or “biomarker.”

4.2 Why bulk covariance is plausible without mechanistic equivalence

Positive tumor covariance can arise because the candidate genes span innate immunity, oxidative stress, mitochondrial regulation, mTOR signaling, and membrane rupture, while the legacy reference is SASP-heavy. Myeloid abundance, stromal remodeling, proliferation, hypoxia, tissue injury, and malignant-

cell fraction can move both summaries together. Gene-wise z scoring does not remove these shared axes. Moreover, two scores derived from the same matrix are not independent anchors; selection, weighting, or testing on shared inputs can inflate apparent concordance [29]. Replication of rho therefore demonstrates cross-cohort covariance, not specificity for either death or senescence. Direct composition adjustment partly addressed this concern: EPIC-based control for immune, fibroblast, and purity fractions attenuated the TCGA covariance by roughly half without eliminating it, and left the GSE39582 covariance unchanged. Cell composition therefore contributes to, but does not fully explain, the covariance, and the composition contribution is cohort-dependent.

The same distinction applies to expression-based drug prediction. When both an exposure score and predicted response are functions of the same transcriptome, their correlation can reflect a shared global expression state even if the predictor ranks responses within its training domain. Observed response in independent cell lines was therefore treated as the anchoring outcome, while tumor-expression correlations were retained as diagnostics rather than patient-level treatment evidence.

The GSE44076 sign difference may reflect altered coexpression, changing cell mixtures, or both. The absence of a paired proxy increase argues against simple transcriptional activation in tumors, and unrelated healthy donors cannot define a temporal trajectory for the cancer cases.

GTEx adds an anatomical and normalization constraint. All-tissue standardization yielded a null sigmoid and positive transverse estimate, whereas colon-only standardization yielded positive estimates in both sites. The reference distribution used for z scoring therefore changed apparent site specificity; full-thickness GTEx tissue and lesion-free colonoscopic mucosa are also not interchangeable normal controls.

4.3 Orthogonal validation and the importance of the biological replicate

Panel-disjoint hUSI and SenePy scores addressed feature overlap with the legacy reference [22, 23, 30]. Associations were tested at the sample/patient level with QC, proliferation, inflammation, leave-one-patient-out, and matched-null controls; the nominal epithelial hUSI result did not persist.

The distinction between 63,689 cells and 23 patients is fundamental. Cells from one patient share genotype, exposure, processing, and microenvironment and cannot serve as independent replications of a patient-level hypothesis. Donor-aware analyses are required to avoid pseudoreplication and false discovery in multi-subject single-cell studies [31, 32]. Pseudobulk reduces the nominal sample size but targets between-patient variation.

Pseudobulk is not itself proof of validity, and with 23 patients it has limited power for covariate-rich and leave-one-patient-out analyses. Its value here is that it aligns the estimator with the biological question and reveals the uncertainty hidden by pooled-cell analysis. The matched-panel analysis addresses a different problem: whether a 17-gene set performs more specifically than genes with similar expression

and detection properties. Requiring both donor-aware inference and matched-null specificity therefore tests biological replication and feature-set distinctiveness rather than relying on nominal cell counts.

4.4 Rationale for excluding analyses without identifiable estimands or independent validation

Method selection was determined by whether the available data defined an estimand and an independent validation target. An aging-clock analysis would need age-labelled calibration, a held-out population, and a definition of age acceleration separable from malignancy; 23 patients with limited age information did not meet those conditions. Mendelian randomization of the composite score would require a strong, reproducible score-level instrument or an exposure GWAS, neither of which was available. Gene-level cis-eQTL/cis-pQTL analyses with colocalization and pleiotropy checks remain possible future work, but they would answer gene-specific causal questions rather than validate the current average.

PC1 ordering lacked an independent root, temporal information, or velocity-compatible measurements, and its orientation and tested scores shared information. Observational expression profiles likewise supplied no intervention labels or held-out response for virtual perturbation. Full data-specific diagnostics are provided in Supplementary Information 1, Supplementary Method 9. Perturbation models should be benchmarked against simple baselines and independent ground truth before mechanistic interpretation [26].

Spatial methods are biologically relevant but require spatially resolved inputs [25]. For this mechanism, transcriptomic coordinates should also be linked to mitochondria–plasma-membrane proximity, localized lipid oxidation, permeability or rupture, and a perturbation/rescue design.

Two 2026 resources clarify what a credible immune-aging extension would require. The Chinese Immune Multi-Omics Atlas (CIMA) provides age-, sex-, genetic-, epigenomic-, transcriptomic-, and circulating-metabolic reference data from healthy Chinese peripheral blood [33], while IDEAL-Age predicts donor-level immunological age from single-cell peripheral-blood profiles and was externally evaluated across independent healthy cohorts, including CIMA [34]. Their appropriate role in the present study is as future PBMC calibration and transportability resources, not as direct validation in colorectal tumor tissue. Applying a healthy-PBMC clock to malignant, epithelial, or stromal cells without domain-specific calibration would exchange one construct-validity problem for another.

4.5 Implications for future experiments

The next informative study is prospective phenotype-anchored validation in human CRC organoids or epithelial–myeloid co-cultures. A factorial innate-stimulus-by-metabolic-stress design should include each single stimulus, combined stress, and a mechanistically selected rescue with independent replication. Primary endpoints should quantify mitochondrial position, localized oxidation, membrane permeability, and rupture by live-cell or electron microscopy. Genetic perturbation of mechanistically justified nodes should distinguish pathway dependence from generic oxidative injury.

Rescue should be interpreted at the phenotype level rather than inferred from reversal of a subset of transcripts. The same experiment should include general stress, viability, and inflammatory controls so that any relationship between the proxy and the defining phenotype can be tested for incremental specificity.

The 17-gene proxy should be specified before the experiment and calibrated against measured phenotype intensity in separate training and validation sets. A useful score would require a monotonic relationship with the defining phenotype, coherent induction/rescue behavior, incremental information beyond proliferation, inflammation, composition, and general stress, and transportability across epithelial and immune contexts. If those criteria are not met, feature selection should be repeated against the measured phenotype.

Multiplex imaging or spatial omics can then connect phenotype, cell identity, and neighborhood. Age, inherited susceptibility, prognosis, and treatment response should be examined only after phenotype anchoring. Pharmacogenomic work should use observed responses to prospectively chosen interventions, and clinical prediction requires independent treated cohorts with locked models.

4.6 Strengths

Strengths include a predefined evidence hierarchy; donor-, pair-, patient-, and cell-line-level inference; anatomical and probe-processing sensitivities; continuous adjusted survival models; algebraic auditing; panel-disjoint senescence constructs; matched null sets; observed pharmacogenomic anchoring; multiplicity control; and retention of null findings. Reporting effect sizes and uncertainty rather than dichotomizing solely at $P = 0.05$ is consistent with current statistical guidance [35]. Input hashes, external-code commits, source data, and independent reproduction of 41 result files improve traceability.

4.7 Limitations

The principal limitation is the absence of the defining mitoxyperilysis phenotype in human CRC and the absence of prospective wet-laboratory validation. The 17-gene panel was author curated, and its provenance check used 15 murine macrophage profiles (three per condition); perturbation weights therefore may not transport to human colorectal epithelium. The legacy senescence reference is inflammatory, and cross-platform z scoring cannot remove tissue-layer, probe, or cohort differences. GTEx age is interval coded, GSE44076 healthy donors are unrelated to the cancer cohort, and the single-cell analysis includes only 23 patients. The four-cohort random-effects synthesis had high heterogeneity ($I^2 = 85.1\%$), so its pooled estimate should be interpreted as a summary of directionally positive but heterogeneous covariance rather than a stable common effect.

The CPTAC-2 modality check used only 10/17 proxy and 8/12 reference proteins, with heterogeneous missingness and gene-specific paired sample sizes of 5–96; it cannot establish protein-level construct validity. Genetic projections measure expression rather than genotype, the observed GDSC2 analysis included 46 CRC cell lines, and cell-line pharmacogenomics may not transport to tumors. The oncoPredict rank diagnostics had weak absolute calibration, and clinical covariates were incomplete.

EPIC estimates on the GSE39582 microarray platform are not directly comparable in scale to RNA-seq estimates. The patient-level single-cell covariance was sensitive to the scoring method, with direction and magnitude differences of approximately 0.4–0.6 within compartments (Supplementary Fig. S12) [30]. All human analyses remain retrospective and observational.

5. Conclusions

Across public colon and CRC transcriptomes, an author-curated 17-gene panel behaves as a context-sensitive expression proxy. Its covariance with a legacy senescence-associated score is reproducible in bulk CRC but varies across normal-colon site, normalization scope, and mucosal context, and it does not withstand panel-disjoint patient-level senescence validation. The available evidence does not establish mitoxyperilysis occurrence, cellular senescence, a temporal transition, three independent compartment programs, inherited risk, prognosis, or drug response. Future work should anchor transcriptomics to the defining spatial, oxidative, and lytic phenotype under prospective perturbation and rescue.

Declarations

Acknowledgements

The authors acknowledge the participants and investigators who generated and shared the public datasets used in this study.

Use of generative artificial intelligence and AI-assisted technologies

During preparation of this manuscript, the authors used OpenAI Codex (GPT-5-based; accessed 16–22 August 2026) under author supervision to assist with document-version comparison, code and analysis auditing, implementation of predefined sensitivity checks, figure formatting, and language editing. The authors reviewed and verified all affected code, numerical outputs, figures, references, interpretations, and text, and take full responsibility for the content of the article. All scientific decisions and conclusions were made by the authors. The tool did not generate experimental observations and is not listed as an author.

Author contributions

Pan Sun: Conceptualization, Methodology, Software, Formal analysis, Data curation, Visualization, Writing—original draft, Writing—review and editing. Jinglin Wang: Conceptualization, Methodology, Validation, Investigation, Writing—original draft, Writing—review and editing. Yao Wang: Software, Formal analysis, Validation. Yan Zhang: Data curation, Validation. Yao Tang: Data curation, Investigation. Juan Yang: Conceptualization, Funding acquisition, Project administration, Supervision, Writing—review and

editing. Zejun Wang: Conceptualization, Resources, Project administration, Supervision, Writing—review and editing. All authors reviewed and approved the final manuscript and agreed to the author order.

Funding

This work was supported by the National Natural Science Foundation of China (grant no. 82360467) and the Science and Technology Fund Projects of the Guizhou Provincial Science and Technology Program (grant nos. QKH JC-ZK [2023]-358 and QKH JC-ZK [2023]-348). The funders had no role in study design, data collection and analysis, decision to publish, or preparation of the manuscript.

Data availability

All primary datasets analysed in this study are publicly available from GTEx, TCGA/UCSC Xena, GEO (GSE235046, GSE63577, GSE44076, GSE39582, and GSE132465), cBioPortal/CPTAC (coad_cptac_2019), DepMap 24Q2, the Human Protein Atlas, the Law et al. colorectal cancer fine-mapping resource, and the official GDSC2/oncoPredict distribution, as detailed in the Methods. Derived numerical data supporting the reported findings are provided in Supplementary Data 1 and in the archived reproducibility package at Zenodo (https://doi.org/10.5281/zenodo.22051069) [40].

Code availability

Author-generated analysis code, frozen analysis contracts, input checksums, software-session records, and figure-source data are archived at Zenodo (version 8.0.0; https://doi.org/10.5281/zenodo.22051069) [40]. The corresponding version-controlled release is available at https://github.com/wangjinglin0905-gif/mitoxyperilysis-crc-evidence-chain/releases/tag/v8.0.0.

Ethics approval and consent to participate

This study involved secondary analysis of publicly available, de-identified datasets only and included no new participant recruitment, intervention, or specimen collection. Ethics approvals and consent procedures were those reported by the original data-generating studies. No additional ethics approval or consent to participate was required for the present secondary analysis.

Consent for publication

Not applicable. No identifiable individual-level information is reported.

Competing interests

The authors declare that they have no competing interests.

References

1. Bray F, Laversanne M, Sung H, et al. Global cancer statistics 2022: GLOBOCAN estimates of incidence and mortality worldwide for 36 cancers in 185 countries. CA Cancer J Clin. 2024;74:229–63. https://doi.org/10.3322/caac.21834.
2. López-Otín C, Blasco MA, Partridge L, et al. Hallmarks of aging: An expanding universe. Cell. 2023;186:243–78. https://doi.org/10.1016/j.cell.2022.11.001.
3. Campisi J. Aging, cellular senescence, and cancer. Annu Rev Physiol. 2013;75:685–705. https://doi.org/10.1146/annurev-physiol-030212-183653.
4. Coppé JP, Desprez PY, Krtolica A, et al. The senescence-associated secretory phenotype: the dark side of tumor suppression. Annu Rev Pathol. 2010;5:99–118. https://doi.org/10.1146/annurev-pathol-121808-102144.
5. Childs BG, Durik M, Baker DJ, et al. Cellular senescence in aging and age-related disease: from mechanisms to therapy. Nat Med. 2015;21:1424–35. https://doi.org/10.1038/nm.4000.
6. Galluzzi L, Vitale I, Aaronson SA, et al. Molecular mechanisms of cell death: recommendations of the Nomenclature Committee on Cell Death 2018. Cell Death Differ. 2018;25:486–541. https://doi.org/10.1038/s41418-017-0012-4.
7. Kayagaki N, Kornfeld OS, Lee BL, et al. NINJ1 mediates plasma membrane rupture during lytic cell death. Nature. 2021;591:131–6. https://doi.org/10.1038/s41586-021-03218-7.
8. Wang Y, Lu J, Carisey AF, et al. Innate immune and metabolic signals induce mitochondria-dependent membrane lysis via mitoxyperiosis. Cell. 2025;188:7155–e717425. https://doi.org/10.1016/j.cell.2025.11.002.
9. Casadio M. Mitoxyperilysis as a distinct cell death type. Nat Cell Biol. 2026;28:1. https://doi.org/10.1038/s41556-025-01861-0.
10. Zhang Y, Sun B, Lin J, et al. A mitoxyperilysis-related signature stratifies prognosis and identifies an aggressive colorectal cancer ecosystem with immune remodeling. Front Cell Dev Biol. 2026;14:1851988. https://doi.org/10.3389/fcell.2026.1851988.
11. Benjamini Y, Hochberg Y. Controlling the false discovery rate: a practical and powerful approach to multiple testing. J R Stat Soc Ser B. 1995;57:289–300. https://doi.org/10.1111/j.2517-6161.1995.tb02031.x.
12. GTEx Consortium. The GTEx Consortium atlas of genetic regulatory effects across human tissues. Science. 2020;369:1318–30. https://doi.org/10.1126/science.aaz1776.
13. Cancer Genome Atlas Network. Comprehensive molecular characterization of human colon and rectal cancer. Nature. 2012;487:330–7. https://doi.org/10.1038/nature11252.
14. Goldman MJ, Craft B, Hastie M, et al. Visualizing and interpreting cancer genomics data via the Xena platform. Nat Biotechnol. 2020;38:675–8. https://doi.org/10.1038/s41587-020-0546-8.

15. Marthandan S, Baumgart M, Priebe S, et al. Conserved senescence-associated genes and pathways in primary human fibroblasts detected by RNA-seq. PLoS ONE. 2016;11:e0154531. https://doi.org/10.1371/journal.pone.0154531.
16. Lee HO, Hong Y, Etlioglu HE, et al. Lineage-dependent gene expression programs influence the immune landscape of colorectal cancer. Nat Genet. 2020;52:594–603. https://doi.org/10.1038/s41588-020-0636-z.
17. Marisa L, de Reyniès A, Duval A, et al. Gene expression classification of colon cancer into molecular subtypes: characterization, validation, and prognostic value. PLoS Med. 2013;10:e1001453. https://doi.org/10.1371/journal.pmed.1001453.
18. Sanz-Pamplona R, Berenguer A, Cordero D, et al. Aberrant gene expression in mucosa adjacent to tumor reveals a molecular crosstalk in colon cancer. Mol Cancer. 2014;13:46. https://doi.org/10.1186/1476-4598-13-46.
19. Yang W, Soares J, Greninger P, et al. Genomics of Drug Sensitivity in Cancer (GDSC): a resource for therapeutic biomarker discovery in cancer cells. Nucleic Acids Res. 2013;41:D955–61. https://doi.org/10.1093/nar/gks1111.
20. Iorio F, Knijnenburg TA, Vis DJ, et al. A landscape of pharmacogenomic interactions in cancer. Cell. 2016;166:740–54. https://doi.org/10.1016/j.cell.2016.06.017.
21. Maeser D, Gruener RF, Huang RS. oncoPredict: an R package for predicting in vivo or cancer patient drug response and biomarkers from cell-line screening data. Brief Bioinform. 2021;22:bbab260. https://doi.org/10.1093/bib/bbab260.
22. Wang J, Zhou X, Yu P, et al. A transcriptome-based human universal senescence index (hUSI) robustly predicts cellular senescence under various conditions. Nat Aging. 2025;5:1159–75. https://doi.org/10.1038/s43587-025-00886-2.
23. Sanborn MA, Wang X, Gao S, et al. Unveiling the cell-type-specific landscape of cellular senescence through single-cell transcriptomics using SenePy. Nat Commun. 2025;16:1884. https://doi.org/10.1038/s41467-025-57047-7.
24. Law PJ, Studd J, Smith J, et al. Systematic prioritization of functional variants and effector genes underlying colorectal cancer risk. Nat Genet. 2024;56:2104–11. https://doi.org/10.1038/s41588-024-01900-w.
25. Singhal V, Chou N, Lee J, et al. BANKSY unifies cell typing and tissue domain segmentation for scalable spatial omics data analysis. Nat Genet. 2024;56:431–41. https://doi.org/10.1038/s41588-024-01664-3.
26. Ahlmann-Eltze C, Huber W, Anders S. Deep-learning-based gene perturbation effect prediction does not yet outperform simple linear baselines. Nat Methods. 2025;22:1657–61. https://doi.org/10.1038/s41592-025-02772-6.
27. Cronbach LJ, Meehl PE. Construct validity in psychological tests. Psychol Bull. 1955;52:281–302. https://doi.org/10.1037/h0040957.

28. Pepe MS, Etzioni R, Feng Z, et al. Phases of biomarker development for early detection of cancer. J Natl Cancer Inst. 2001;93:1054–61. https://doi.org/10.1093/jnci/93.14.1054.
29. Kriegeskorte N, Simmons WK, Bellgowan PSF, Baker CI. Circular analysis in systems neuroscience: the dangers of double dipping. Nat Neurosci. 2009;12:535–40. https://doi.org/10.1038/nn.2303.
30. Noureen N, Ye Z, Chen Y, Wang X, Zheng S. Signature-scoring methods developed for bulk samples are not adequate for cancer single-cell RNA sequencing data. eLife. 2022;11:e71994. https://doi.org/10.7554/eLife.71994.
31. Zimmerman KD, Espeland MA, Langefeld CD. A practical solution to pseudoreplication bias in single-cell studies. Nat Commun. 2021;12:738. https://doi.org/10.1038/s41467-021-21038-1.
32. Squair JW, Gautier M, Kathe C, et al. Confronting false discoveries in single-cell differential expression. Nat Commun. 2021;12:5692. https://doi.org/10.1038/s41467-021-25960-2.
33. Yin J, Zheng Y, Huang Z, et al. Chinese Immune Multi-Omics Atlas. Science. 2026;391:eadt3130. https://doi.org/10.1126/science.adt3130.
34. Xu Y, Luo Z, He K, et al. IDEAL-Age: an interpretable deep learning framework for single-cell resolution profiling of immunological aging. Genome Biol. 2026;27:236. https://doi.org/10.1186/s13059-026-04188-7.
35. Wasserstein RL, Schirm AL, Lazar NA. Moving to a world beyond p < 0.05. Am Stat. 2019;73(sup1):1–19. https://doi.org/10.1080/00031305.2019.1583913.
36. Racle J, de Jonge K, Baumgaertner P, et al. Simultaneous enumeration of cancer and immune cell types from bulk tumor gene expression data. eLife. 2017;6:e26476. https://doi.org/10.7554/eLife.26476.
37. Vasaikar SV, Huang C, Luo X, et al. Proteogenomic analysis of human colon cancer reveals new therapeutic opportunities. Cell. 2019;177:1035–49. https://doi.org/10.1016/j.cell.2019.03.030. .e19.
38. Tsherniak A, Vazquez F, Montgomery PG, et al. Defining a cancer dependency map. Cell. 2017;170:564–76. https://doi.org/10.1016/j.cell.2017.06.010. .e16.
39. Uhlén M, Fagerberg L, Hallström BM, et al. Tissue-based map of the human proteome. Science. 2015;347:1260419. https://doi.org/10.1126/science.1260419.
40. Sun P, Wang J, Wang Y, Zhang Y, Tang Y, Yang J, Wang Z. Mitoxyperilysis CRC evidence chain. Version 8.0.0. Zenodo. 2026. https://doi.org/10.5281/zenodo.22051069

Figures

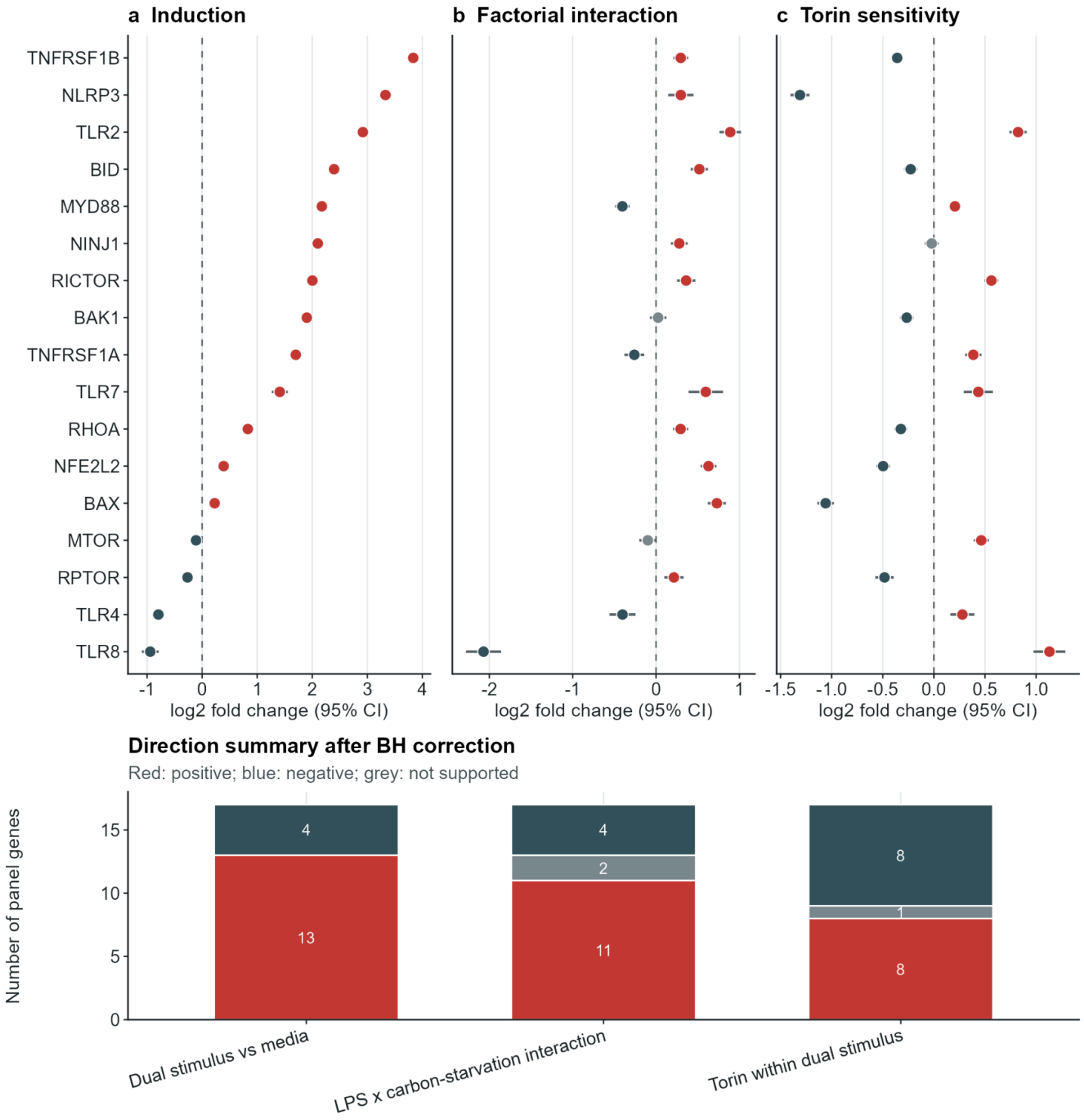


Figure 1

Perturbational response of the 17-gene transcriptomic proxy
(a) Combined lipopolysaccharide (LPS) plus carbon-starvation versus media log2 fold changes for all 17 genes in GSE235046. (b) Formal factorial interaction estimates, combined stress − LPS − carbon starvation + media. (c) Torin-treated versus untreated combined-stress estimates. Points and horizontal lines denote limma-voom estimates and 95% confidence intervals; filled colors indicate direction among

genes with BH q < 0.05. (d) Counts of positive, negative, and null effects for each estimand. TMM normalization, robust empirical-Bayes modeling, and BH correction were applied separately across the 17 genes in each contrast. The independent unit was the culture/sample (three per condition). Bidirectional effects and the absence of coherent Torin reversal support context responsiveness but not a validated activity-and-rescue signature

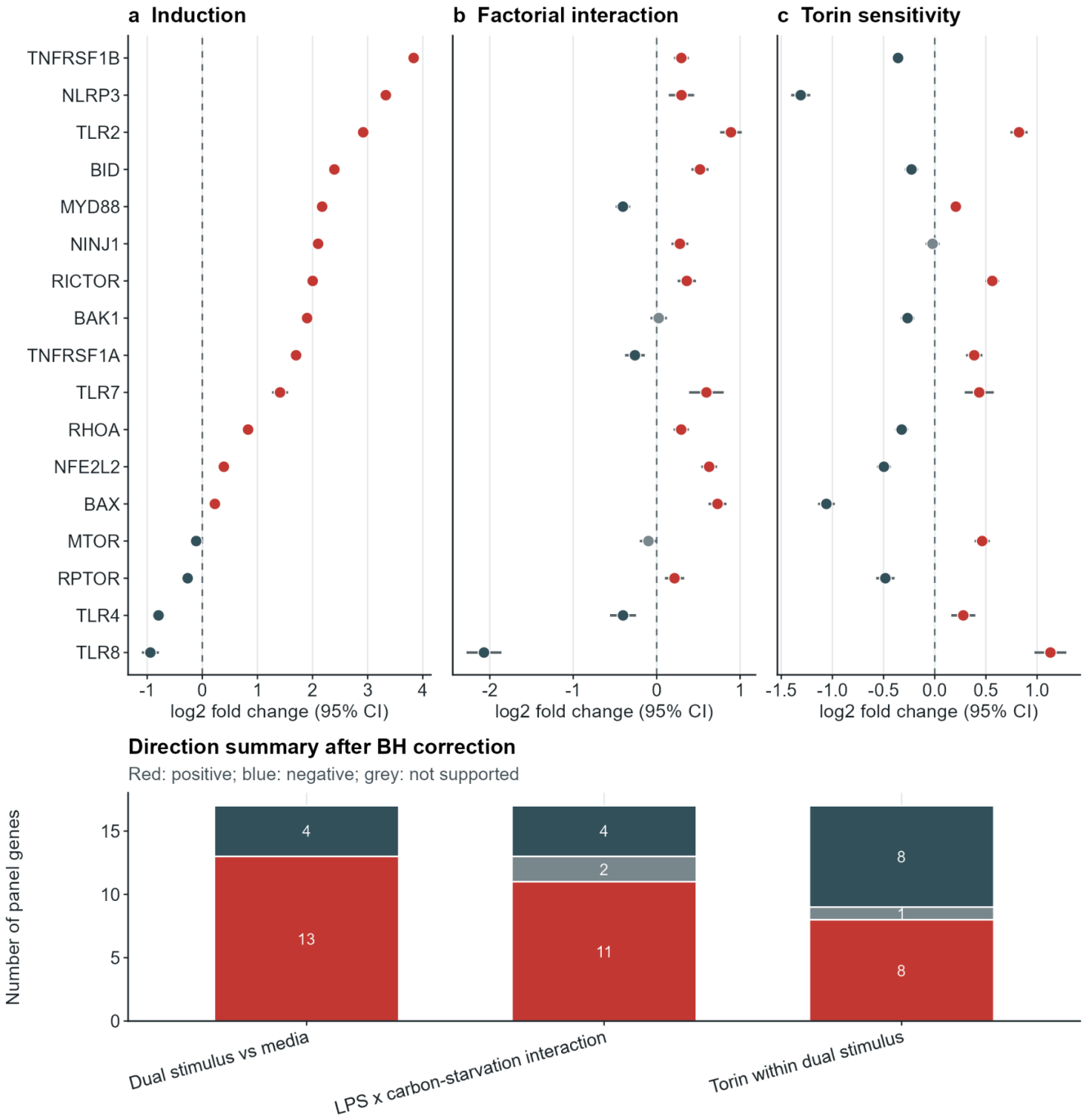


Figure 1

Perturbational response of the 17-gene transcriptomic proxy
(a) Combined lipopolysaccharide (LPS) plus carbon-starvation versus media log2 fold changes for all 17 genes in GSE235046. (b) Formal factorial interaction estimates, combined stress − LPS − carbon starvation + media. (c) Torin-treated versus untreated combined-stress estimates. Points and horizontal lines denote limma-voom estimates and 95% confidence intervals; filled colors indicate direction among genes with BH q < 0.05. (d) Counts of positive, negative, and null effects for each estimand. TMM normalization, robust empirical-Bayes modeling, and BH correction were applied separately across the 17 genes in each contrast. The independent unit was the culture/sample (three per condition). Bidirectional effects and the absence of coherent Torin reversal support context responsiveness but not a validated activity-and-rescue signature

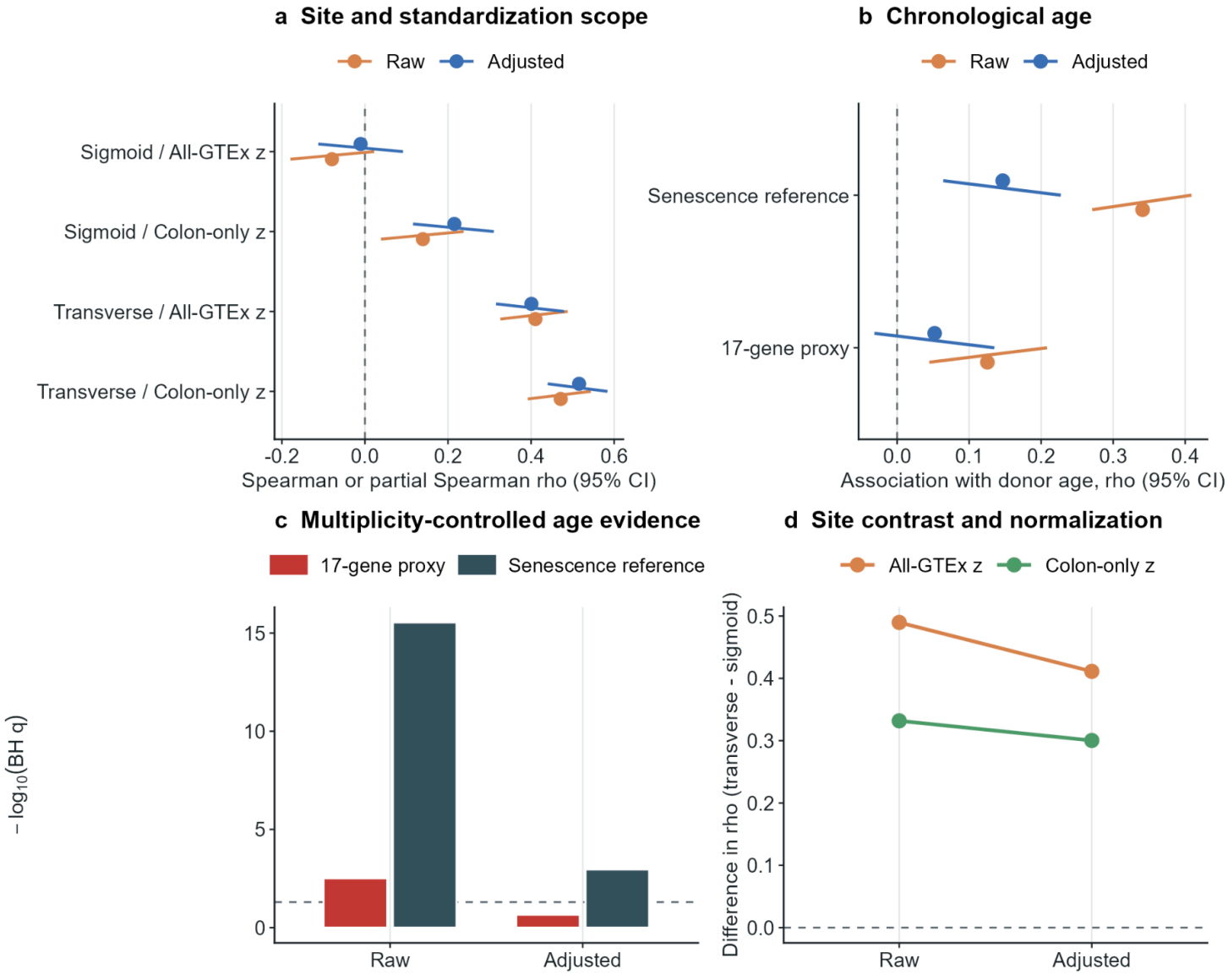


Figure 2

Normal-colon anatomy, normalization scope, and chronological age
(a) Proxy–legacy-senescence-reference correlations in donor-level sigmoid and transverse GTEx colon

under all-GTEx versus colon-only gene standardization; raw and covariate-adjusted estimates are shown. (b) Proxy–age association before and after adjustment for MKI67, sex, and number of sampled sites. (c) Corresponding legacy-reference–age estimates. (d) Difference between transverse and sigmoid estimates under each standardization scope. Horizontal lines denote 95% confidence intervals where available. The donor was the independent unit. Site and the reference population used for gene standardization materially affect interpretation

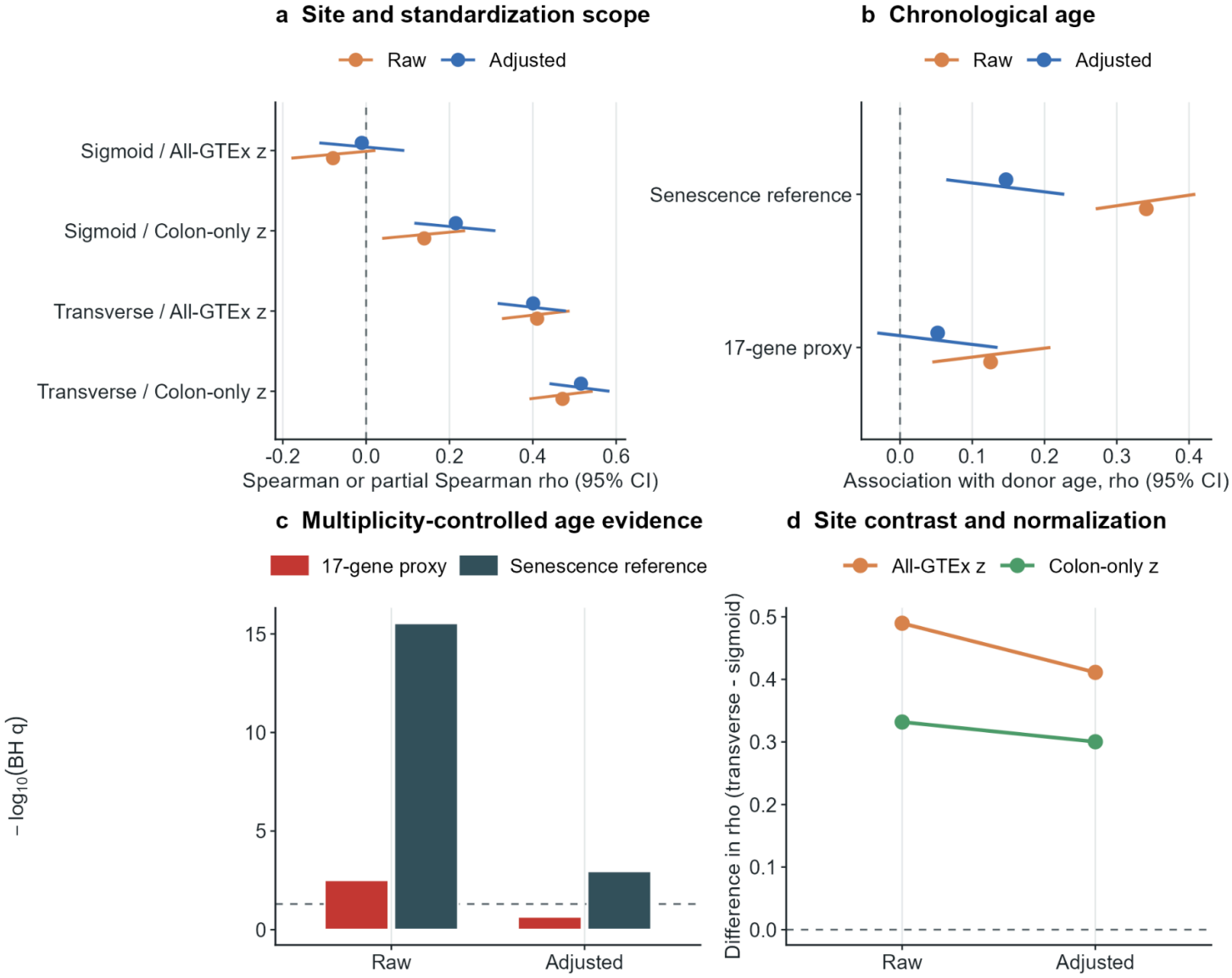


Figure 2

Normal-colon anatomy, normalization scope, and chronological age
(a) Proxy–legacy-senescence-reference correlations in donor-level sigmoid and transverse GTEx colon under all-GTEx versus colon-only gene standardization; raw and covariate-adjusted estimates are shown. (b) Proxy–age association before and after adjustment for MKI67, sex, and number of sampled sites. (c) Corresponding legacy-reference–age estimates. (d) Difference between transverse and sigmoid estimates under each standardization scope. Horizontal lines denote 95% confidence intervals where

available. The donor was the independent unit. Site and the reference population used for gene standardization materially affect interpretation

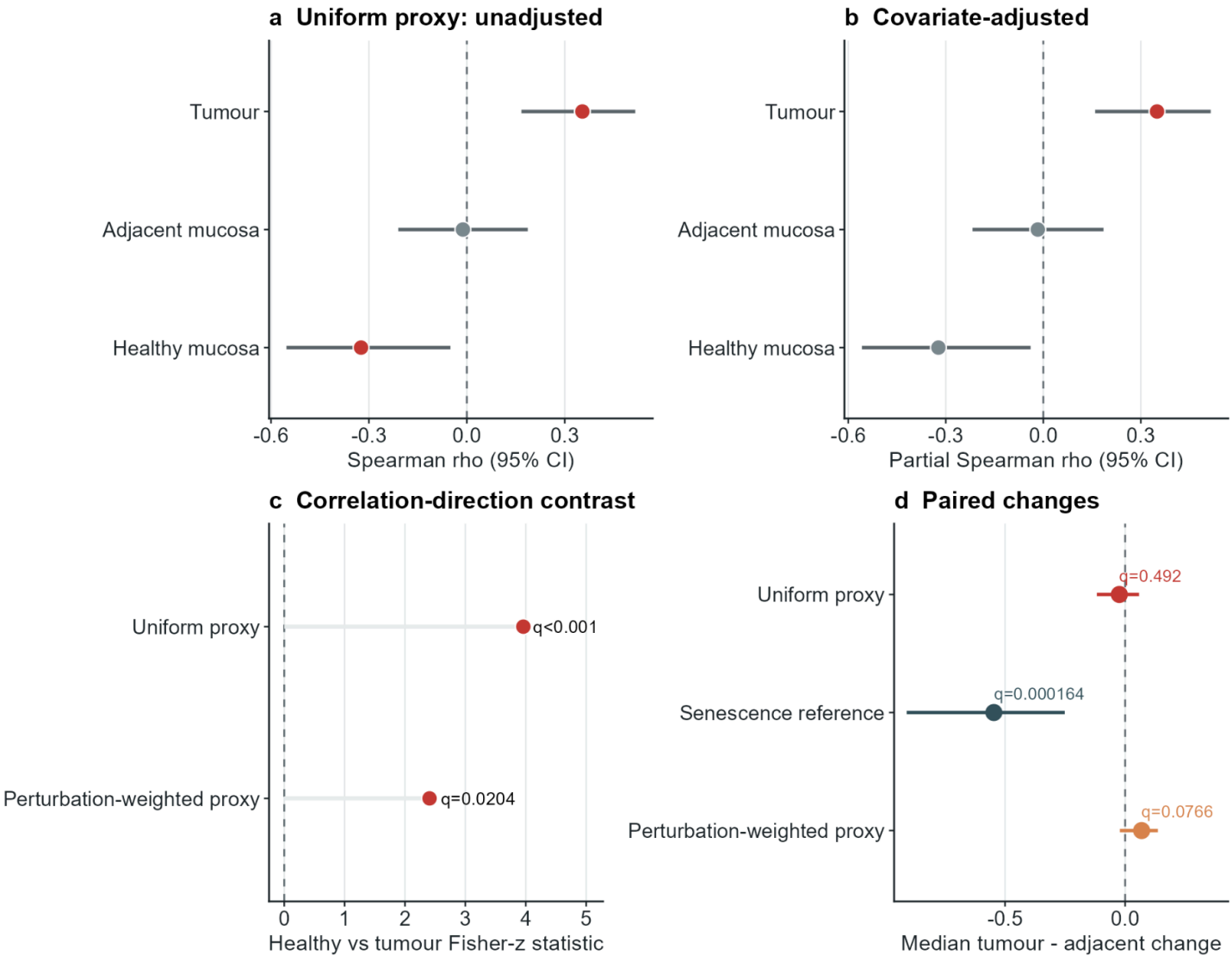


Figure 3

Context-dependent covariance across healthy, adjacent, and tumor mucosa
(a) Corrected probe-aggregated raw Spearman correlations in GSE44076. (b) Covariate-adjusted partial correlations. (c) Fisher-z correlation differences between tissue contexts. (d) Paired tumor-minus-adjacent score changes in 98 CRC participants. Healthy mucosa came from 50 unrelated donors and was not paired with the cancer cohort. BH-adjusted q values are displayed. The supported finding is a correlation-sign difference between healthy mucosa and tumor, not a temporal healthy-to-tumor sequence

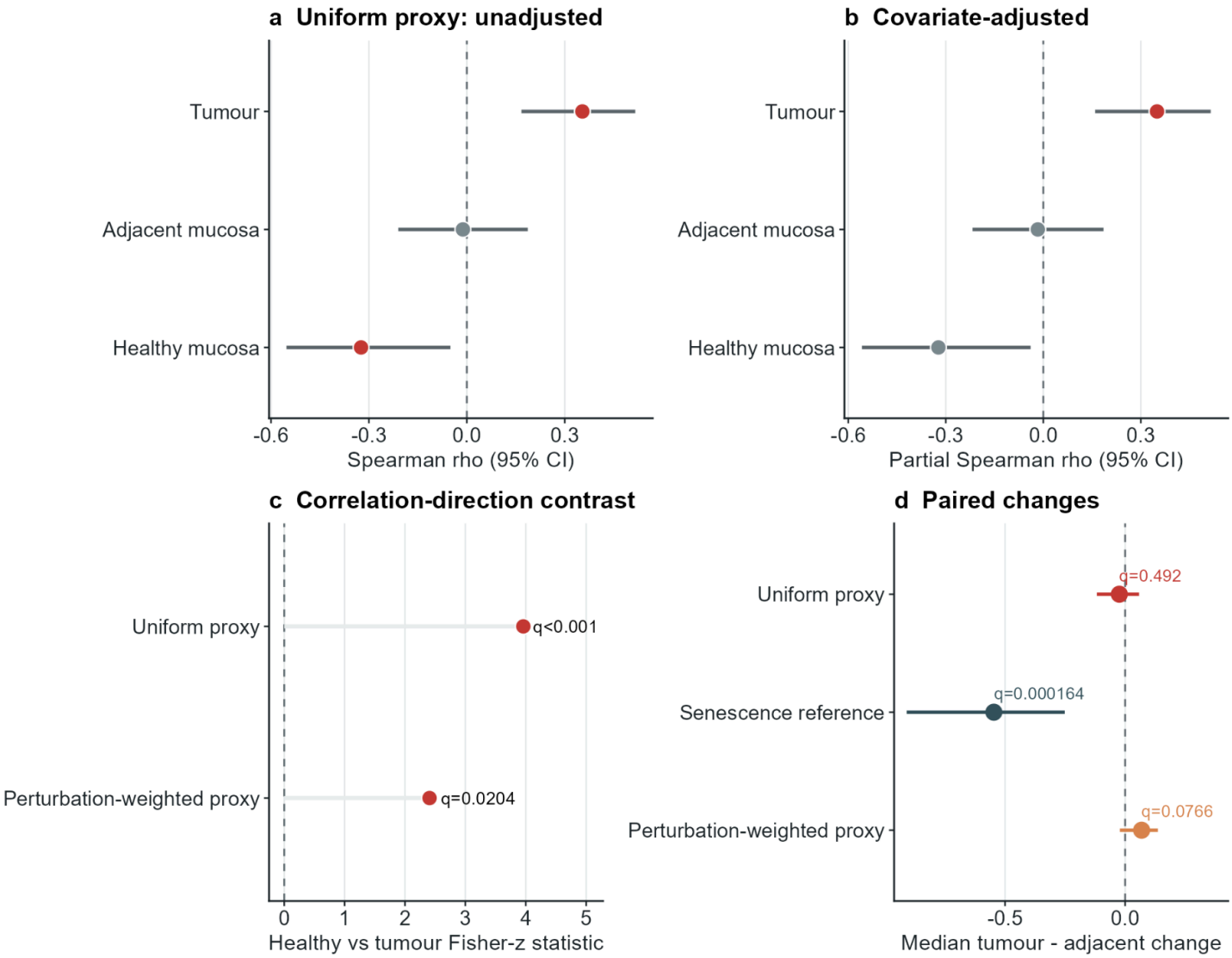


Figure 3

Context-dependent covariance across healthy, adjacent, and tumor mucosa
(a) Corrected probe-aggregated raw Spearman correlations in GSE44076. (b) Covariate-adjusted partial correlations. (c) Fisher-z correlation differences between tissue contexts. (d) Paired tumor-minus-adjacent score changes in 98 CRC participants. Healthy mucosa came from 50 unrelated donors and was not paired with the cancer cohort. BH-adjusted q values are displayed. The supported finding is a correlation-sign difference between healthy mucosa and tumor, not a temporal healthy-to-tumor sequence

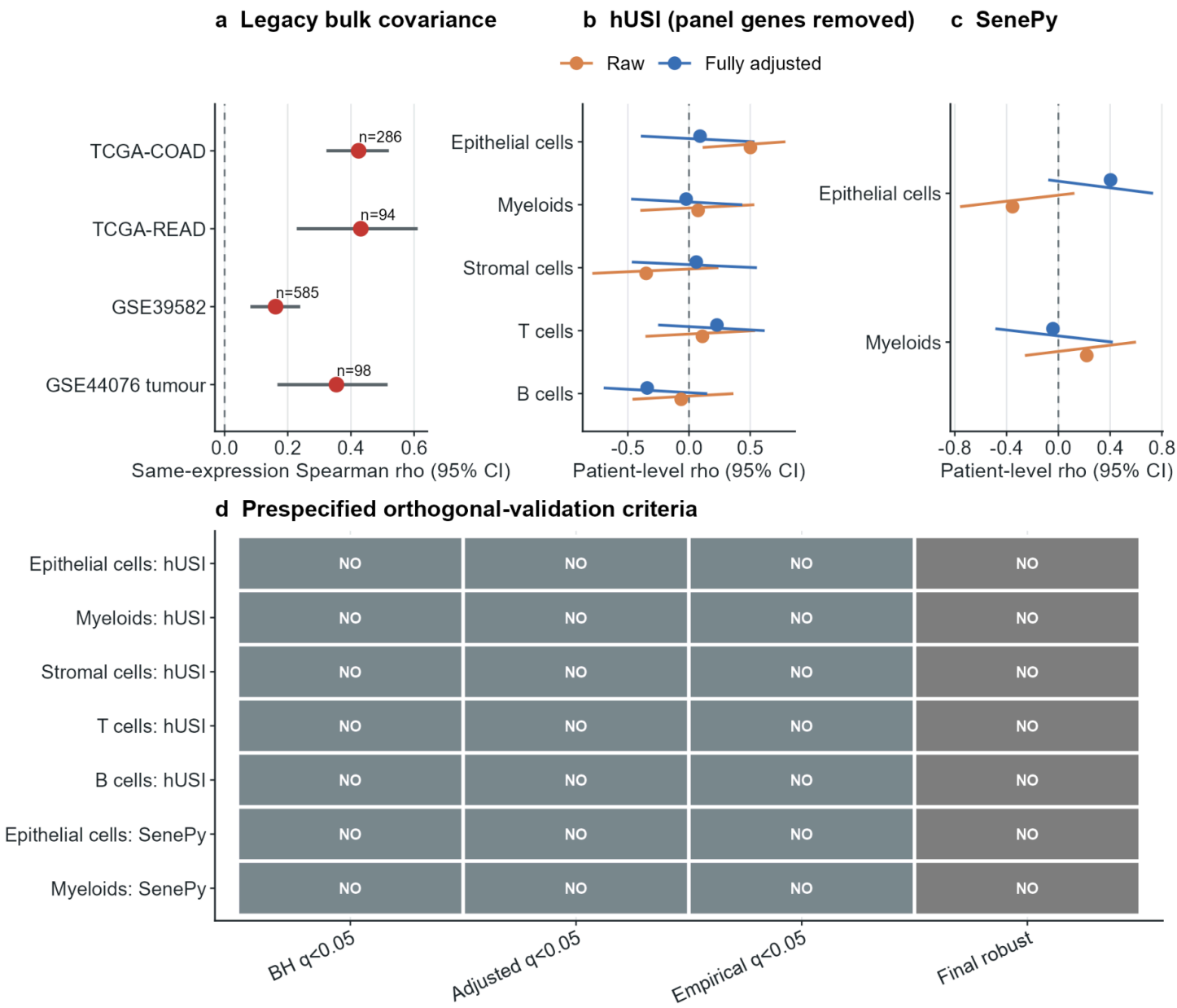


Figure 4

Bulk covariance and orthogonal patient-level senescence validation
(a) Same-expression proxy–legacy-reference correlations in bulk CRC cohorts. (b) Raw and fully adjusted patient-level associations with panel-disjoint hUSI across GSE132465 cell compartments. (c) Corresponding SenePy intestine/epithelial and intestine/macrophage results. (d) Prespecified seven-test decision matrix incorporating BH correction, full covariate adjustment, leave-one-patient-out stability, and expression/detection-matched random-panel specificity. Tumor sample-by-cell-type profiles with at least 20 cells were analyzed; patients/specimens, not cells, determined sample size. No orthogonal test met the complete validation criterion

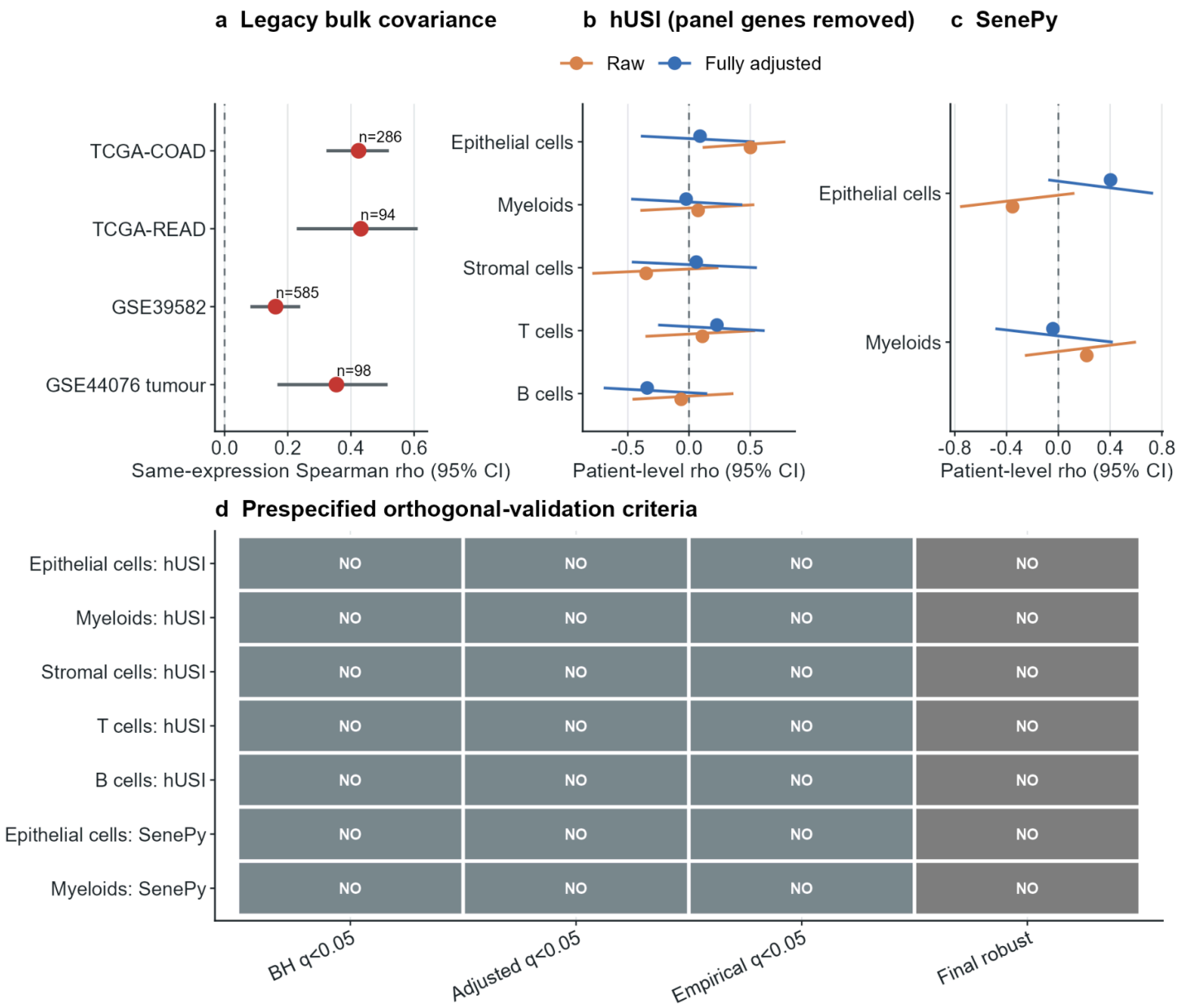


Figure 4

Bulk covariance and orthogonal patient-level senescence validation
(a) Same-expression proxy–legacy-reference correlations in bulk CRC cohorts. (b) Raw and fully adjusted patient-level associations with panel-disjoint hUSI across GSE132465 cell compartments. (c) Corresponding SenePy intestine/epithelial and intestine/macrophage results. (d) Prespecified seven-test decision matrix incorporating BH correction, full covariate adjustment, leave-one-patient-out stability, and expression/detection-matched random-panel specificity. Tumor sample-by-cell-type profiles with at least 20 cells were analyzed; patients/specimens, not cells, determined sample size. No orthogonal test met the complete validation criterion

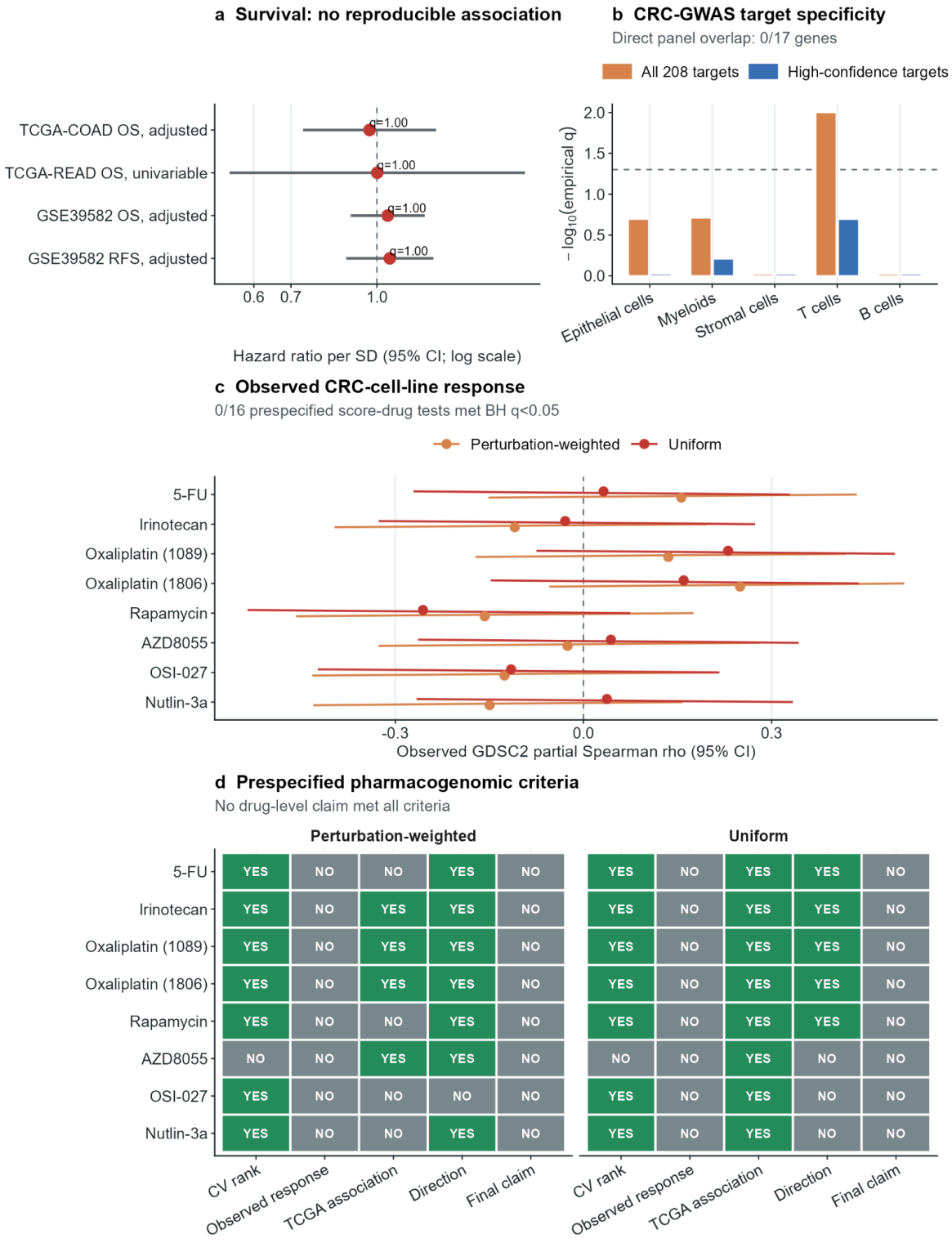


Figure 5

Evidence boundaries for prognosis, genetics, and drug response
(a) Continuous per-SD Cox estimates for TCGA and GSE39582 overall survival/relapse-free survival, with 95% confidence intervals. (b) Direct overlap and matched-null specificity results for 2024 CRC target-gene projections. (c) Raw and fully adjusted associations between the proxies and observed ln(IC50) for eight prespecified drugs in 46 GDSC2 CRC cell lines. (d) Evidence-gate matrix combining oncoPredict

out-of-fold rank performance, absolute calibration, observed-response support, TCGA predicted association, and final claim status. No prognostic, genetic-specificity, or drug-level claim passed the complete prespecified gate

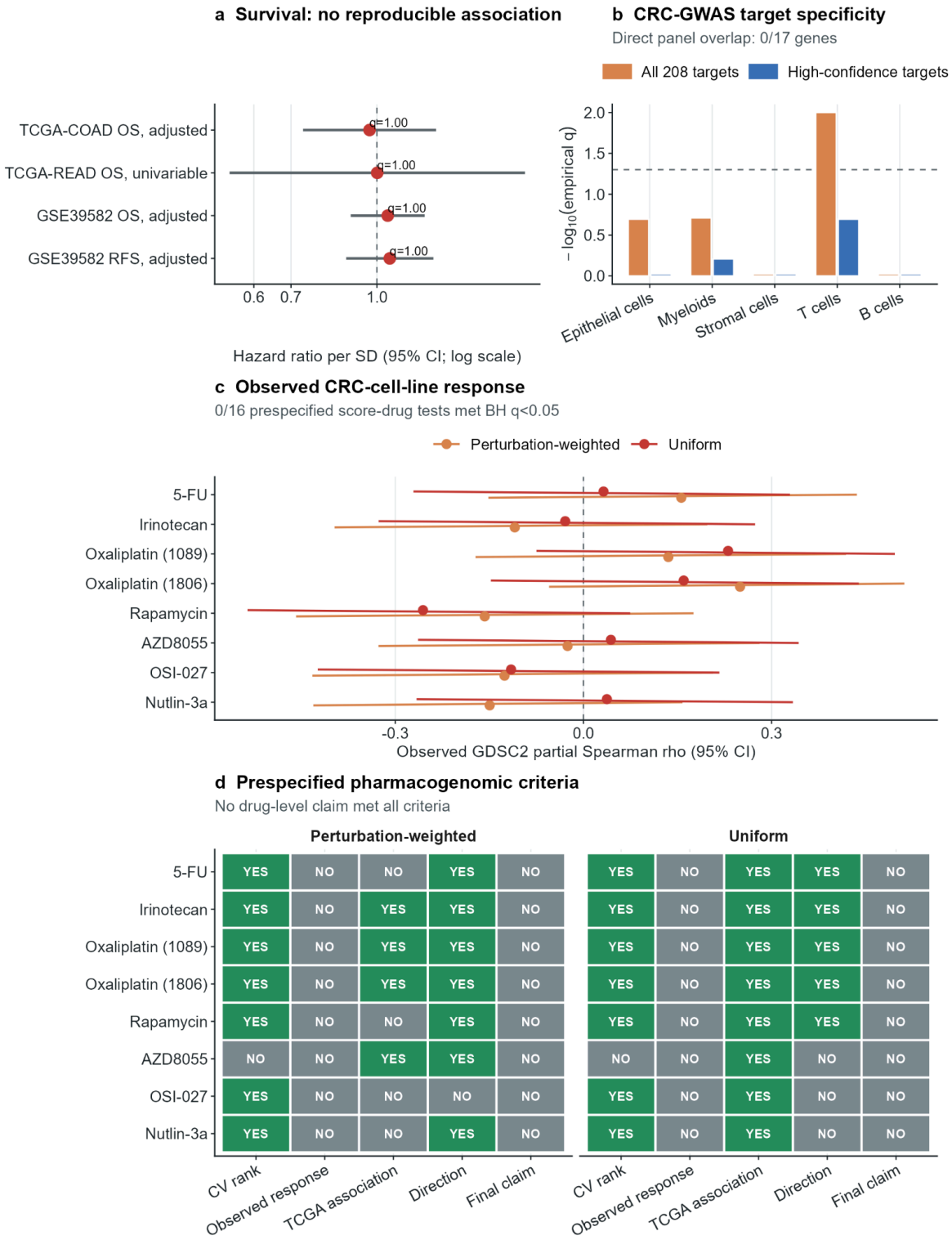


Figure 5

Evidence boundaries for prognosis, genetics, and drug response
(a) Continuous per-SD Cox estimates for TCGA and GSE39582 overall survival/relapse-free survival, with 95% confidence intervals. (b) Direct overlap and matched-null specificity results for 2024 CRC target-gene projections. (c) Raw and fully adjusted associations between the proxies and observed ln(IC50) for eight prespecified drugs in 46 GDSC2 CRC cell lines. (d) Evidence-gate matrix combining oncoPredict out-of-fold rank performance, absolute calibration, observed-response support, TCGA predicted association, and final claim status. No prognostic, genetic-specificity, or drug-level claim passed the complete prespecified gate

Supplementary Files

This is a list of supplementary files associated with this preprint. Click to download.

- SupplementaryFig.S1.pdf
- SupplementaryFig.S1.pdf
- SupplementaryFig.S10.pdf
- SupplementaryFig.S10.pdf
- SupplementaryFig.S3.pdf
- SupplementaryFig.S3.pdf
- SupplementaryFig.S11.pdf
- SupplementaryFig.S11.pdf
- SupplementaryFig.S12.pdf
- SupplementaryFig.S12.pdf
- SupplementaryFig.S2.pdf
- SupplementaryFig.S2.pdf
- SupplementaryFig.S4.pdf
- SupplementaryFig.S4.pdf
- SupplementaryFig.S5.pdf
- SupplementaryFig.S5.pdf
- SupplementaryFig.S6.pdf
- SupplementaryFig.S6.pdf
- SupplementaryFig.S7.pdf
- SupplementaryFig.S7.pdf
- SupplementaryFig.S8.pdf
- SupplementaryFig.S8.pdf
- SupplementaryFig.S9.pdf

- SupplementaryFig.S9.pdf
- SupplementaryData1.xlsx
- SupplementaryData1.xlsx
- SupplementaryFile1ReproducibilityPackage.zip
- SupplementaryFile1ReproducibilityPackage.zip
- SupplementaryInformation1.docx
- SupplementaryInformation1.docx